REMOTE SENSING AND GOOGLE EARTH ENGINE FOR RAPID FLOOD MAPPING AND DAMAGE ASSESSMENT: A CASE OF TYPHOON GONI (ROLLY) AND VAMCO (ULYSSES)

R. D. Tumaneng [1*], K. E. R. Morico [2], J. A. Principe [3]

[1] DOST-Philippine Council for Industry, Energy and Emerging Technology Research and Development, Taguig City, Philippines – roven.tumaneng@pcieerd.dost.gov.ph
[2] DOST-Advanced Science and Technology Institute, Quezon City, Philippines – korinneella.morico@asti.dost.gov.ph
[3] Dept. of Geodetic Engineering, University of the Philippines Diliman, Quezon City, Philippines – japrincipe@up.edu.ph

KEY WORDS: Google Earth Engine, SAR, typhoon, flood mapping, damage assessment

ABSTRACT:

Flooding is a devastating natural disaster with global repercussions, affecting human life, crop production, and infrastructure. The increasing frequency and unpredictability of flood events, driven by climate change, highlight the urgent need for rapid and accurate flood mapping and damage assessment. This study explores the use of Google Earth Engine, a web-based platform that utilizes satellite imagery and geospatial data, for flood mapping and damage assessment. By incorporating localized datasets, such as region-specific land cover maps and population density information, the developed workflow provides a robust tool for assessing flood extent, identifying high-risk areas, and estimating the impact on cropland and urban centers. Key findings showed that Cagayan province presented the highest potential flood area, covering approximately 55,063 hectares. This province also had the largest population at risk, with around 39,440 individuals potentially exposed to the effects of flooding. Moreover, the cropland in Cagayan province experienced the most substantial impact, with around 91.26% being affected due to the swelling of the Cagayan River. Camarines Sur experienced severe devastation in urban areas, with about 269 hectares affected by flooding from the Bicol River. This study's findings contribute to a comprehensive understanding of flood impacts beyond the extent of flooding, facilitating informed decision-making, emergency response planning, and targeted interventions to mitigate the effects of floods on communities, agriculture, and urban areas. The approach presented here can be applied in other regions, supporting improved flood management and mitigation strategies for national.

1. INTRODUCTION

1.1 Background of the study

In recent years, the frequency and intensity of flooding events, which are one of the world's most common natural disasters, have posed significant challenges to communities worldwide. Floods have had significant negative global impacts on human life, crop production, and infrastructure. Due to climate change, flood occurrences are becoming more frequent and less predictable (Pralle 2019). Rapid and accurate flood mapping and damage assessment are crucial for effective emergency response, relief efforts, and urban planning. With the advent of advanced technologies and the power of geospatial data, one notable development in the field of disaster risk reduction and management (DRRM) is the utilization of Google Earth Engine (GEE).

GEE is a web-based platform that leverages satellite imagery and geospatial data, has revolutionized the way we visualize and analyze our planet (Tamiminia et al., 2020). With a comprehensive collection of datasets and with a powerful set of computation tools that can be used for various geospatial analysis and remote sensing applications, this platform offers a powerful tool for assessing flood extent and identifying areas at risk (Gorelick et al., 2017). In addition to satellite imagery, Google Earth Engine also provides access to other types of geospatial data, such as climate data, land cover maps, elevation data, and more.

With GEE, the need to download large and complex data has been eliminated, and all necessary analyses can be completed without additional storage and processing requirements on the end user's end. The platform also provides large scale visualization and analysis of geospatial data, particularly Sentinel-1 Synthetic Aperture Radar (SAR) imagery (Gorelick et al., 2017). The utilization of SAR for flood mapping stands as standard and reliable approach for determining the extent of major floods (Voigt, et al., 2007; Tay et al., 2020).

SAR operates as an active sensor, utilizing the microwave band within the broad radio spectrum. It offers the advantage of day-and-night imaging capabilities and the ability to penetrate cloud cover and, to some extent, rain (Nghia et al., 2022) These distinct characteristics make SAR a valuable tool for flood mapping, enabling frequent observations regardless of weather conditions or time of day (Franceschetti and Lanari, 1999; Marzano et al., 2011; Schumann et al., 2009; O'Grady et al., 2011). Moreover, its effectiveness is further enhanced by incorporating localized datasets specific to the region of interest.

Localized datasets can include information such as local topography, land use maps, floodplain boundaries, and drainage systems, rainfall data and even population data. These datasets offer valuable insights on the characteristics and impact of flooding events in a specific region. By incorporating this localized information to flood mapping and damage assessment, emergency responders and decision-makers can make informed decisions on evacuation routes, resource allocation, and recovery strategies.

*Corresponding author

The potential of Google Earth Engine to provide a rapid flood extent mapping and damage assessment using SAR data and localized dataset is explored in the study. Such localized dataset includes the latest Land Cover Maps (LCM) produced by the National Mapping and Resource Information Authority (NAMRIA) of the Department of Environment and Natural Resources (DENR) and the High-Resolution Population Density Maps from United Nations Office for the Coordination of Humanitarian Affairs (UN OCHA). The objective of this study is to generate a flood extent map for the assessment of affected areas in the Philippines using a change detection approach on Sentinel-1 (SAR) data through Google Earth Engine following the recommended practice of UN SPIDER (United Nations Platform for Space-based Information for Disaster Management and Emergency Response). The study also aims to provide a detailed representation of the affected areas, ranging from individual barangays to entire regions, by employing a regions-specific dataset. Moreover, this study also introduces a flood delineation technique that requires minimal human intervention and is viable for operation on a national scale. The suggested approach can generate flood maps in near-real time (NRT) particularly in the aftermath of typhoon-related events as well as to determine the possible affected cropland areas, urban areas, and population. The output map and shapefiles can be used by relevant stakeholders including government agencies that are mandated to manage emergency response operations.

1.2 Typhoon Goni and Vamco

Super Typhoon Goni visited the Philippines on 1 November 2020 and was considered the strongest tropical cyclone during that year. Typhoon Goni brought intense rainfall, strong winds, mudslides, and storm surges to Luzon Island (Fig. 1).

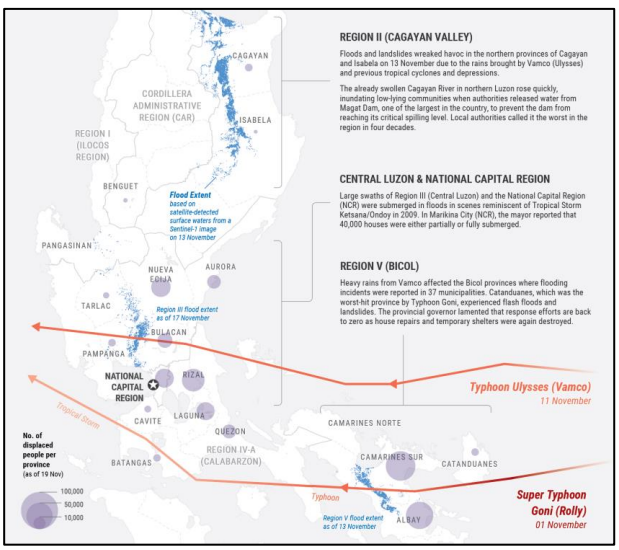

Figure 1. Tracks of Super Typhoon Rolly and Typhoon Ulysses (UN OCHA, 2020)

Subsequently, Tropical Storms Atsani *(Siony)* and Etau *(Tonyo)* made landfall in Luzon and Visayas between 5 to 8 November. Shortly after, a Category-4 Typhoon named Vamco *(Ulysses)* struck central Luzon on 11 and 12 November, resulting in floods in the low-lying suburbs of Manila and triggering floods and landslides in the provinces of Cagayan and Isabela in the northern region, affecting agricultural areas. The heavy rainfall brought by Typhoon Vamco also affected the Bicol provinces, leading to floodings in many municipalities (UN OCHA, 2020).

Table 1 provides a summary of the aftermath of Super Typhoon Goni and Typhoon Vamco, based on the reports from the National Disaster Risk Reduction and Management Council (NDRRMC), and Department of Social Welfare and Development – Disaster Response Operations Monitoring and Information Center - (DSWD - DROMIC).

Category	Super Typhoon Goni *(Rolly)*	Typhoon Vamco *(Ulysses)*
Affected household	803,572 families or 3,355,995 persons were affected in 5,996 barangays	1,262,939 families (5,184,824 people) were affected in 7,827 barangays
Affected regions	NCR, II, III, CALABARZON, MIMAROPA, V, VIII, and CAR (8 Regions, 32 Provinces, 44 Cities and 359 municipalities)	NCR, I, II, III, CALABARZON, MIMAROPA, V and CAR. (8 Regions, 33 Provinces, 58 Cities and 477 municipalities)
Hardest hit area	Camarines Sur, Albay and Catanduanes	Cagayan and Isabela
Casualties and injured	25 dead, 399 injured, 6 missing.	101 people dead, 85 injured, 10 missing
Houses damaged	398,266 damaged houses; of which, 69,576 are totally damaged and 328,690 are partially damaged	209,170 damaged houses; of which 26,510 were totally damaged and 182,660 partially damaged
Damage to infrastructure (estimated)	PHP 12.8 billion	PHP 12.9 billion
Damage to agriculture (estimated)	PHP 5.01 billion	PHP 7.3 billion

Table 1. Summary of the aftermath caused by Super Typhoon Goni and Typhoon Vamco (IFRC, 2020; IFRC, 2021, NDRRMC, 2020; NDRRMC, 2021)

2. METHODOLOGY

2.1 Study Area

2.1.1 Cagayan River Basin: The Cagayan River Basin (CRB) is the largest river basin in the Philippines, situated in the northeastern part of the island of Luzon. CRB is surrounded by natural features, including the Sierra Madre to the east, the Central Cordillera to the west, the Caraballo Mountain ranges to the south, and the Babuyan Channel to the north (Principe, 2012).

As the largest river basin in the Philippines, the CRB encompasses a vast land area of 27,493.49 km^2 (Principe and Blanco, 2012). It encompasses several provinces across three administrative regions, specifically Apayao, Benguet, Ifugao, Kalinga, Mountain Province, and parts of Abra in the Cordillera Administrative Region; Cagayan, Isabela, Nueva Vizcaya, and Quirino in Region 2; as well as sections of Aurora and Nueva Ecija in Region 3. In its entirety, the Cagayan River Basin spans 12 provinces, 122 municipalities/cities, and 2,459 barangays. The river basin is further divided into 23 sub-watersheds, each characterized by distinct hydrological characteristics (UPLB-CFNR, 2018).

Approximately 31.44% of the total land area within the river basin is occupied by annual crops, which spans an estimated area of 864,546 hectares, making it the most extensive land use category in the region (UPLB-CFNR, 2018).

2.1.2 Bicol River Basin: Situated in the southwestern part of Luzon, the Bicol River Basin (BRB) of 317,103 hectares land area passes through the central part of Camarines Sur, the northern part of Albay, and a part of Camarines Norte in the Bicol Region (DENR-RBCO, 2015).

The BRB is characterized by the convergence of two major rivers, namely the Bicol River and the Libmanan River. These rivers meet near Aslong, Libmanan, before eventually emptying into the San Miguel Bay. Considering the topographical features, the watershed delineation identifies 43 local government units (LGUs) that are either fully or partially located within the Bicol River Basin. Furthermore, the river basin is subdivided into eight distinct subwatersheds. Approximately 77% of the basin area, totalling 243,800 hectares, consists of farmed agricultural areas (DENR-RBCO, 2015).

2.2 Data

In this study, we utilized the Sentinel-1 data, which is freely accessible through the European Space Agency (ESA), to map the flood extent in the Cagayan and Bicol River Basins. Sentinel-1 offers data in the C-band (5.4 GHz) with dual-polarization channels (VH and VV) and has a repeat cycle of 12 days. To enhance the accuracy of the flood extent, we also used complementary datasets such as JRC Global Surface water dataset and the WWF HydroSHEDS Digital Elevation Model.

For the assessment of flood damage, we incorporated the land use land cover (LULC) dataset obtained from DENR-NAMRIA and the population dataset from UN OCHA. These datasets were used to evaluate the impact of the floods on the cropland and urban areas and to estimate the number of people potentially affected by the inundation.

2.3 SAR Data and processing

2.3.1 Data Selection: This study used the Level 1 processed Ground Range Detected (GRD) product from the Sentinel-1 satellite. Using the predefined parameters, the entire Sentinel-1 GRD archive, referred to as *ImageCollection* in Google Earth Engine, undergoes filtering based on the instrument mode, the polarization, the pass direction, and the resolution, and is then subsequently snipped to the boundaries of the study area. The filtered *ImageCollection* is then narrowed down to the selected time periods (before and after the flood event).

In terms of acquisition mode, the Interferometric Wide swath (IW) mode was used in this study since this is the main acquisition mode for land surface that satisfies the majority of service requirements with long-term archives (Torres et al., 2012). A spatial resolution of 10 m pixel was chosen for this study, while for the polarization, VH polarization was used since VV polarization may result in overestimation of flooded areas due to its higher backscatter from water surfaces. Further, VV polarization is influenced by vertical structures, while VH polarization is more responsive to changes on the land surface. VH polarization is also better suited for identifying flood-affected areas, as it offers enhanced contrast between flooded and non-flooded areas in SAR images, since VH polarization manifests darker and blacker tones in comparison to VV polarization (Islam and Meng, 2022). Another parameter considered in this study was the pass direction. The pass direction is an important consideration since it determines the path that the satellite takes over a specific area. The ASCENDING pass direction was chosen since this is the only pathway direction available in the study site.

Once the parameters were set, images were then selected through predefined dates. All available Sentinel-1 SAR imageries were used for flood mapping, covering the pre-flood period from February 11 -23, 2020, and post- flooding period from November 1 to November 15, 2020. In order to be guided on the choice of the pre-flood period, the pre-flood coverage date was selected by identifying a period within that specific year with the lowest recorded rainfall, using the data from the Automatic Rain Gauge (ARG) of *PhilSensors* (https://philsensors.asti.dost.gov.ph/), which is managed by the Advanced Science and Technology Institute (ASTI) of the Department of Science and Technology (DOST). This decision was made to ensure that the selected timeframe represents a period when the area was not affected by the other previous flooding incidents.

Once the images were selected based on the predefined dates, a mosaic of the selected tiles will be created and clipped to the study area. In this case, the GADM v4.1 2022 administrative level 1 (province level) were used to clip the study area.

2.3.2 Preprocessing: As Sentinel-1 dataset is stored on the GEE platform, the information derived from Sentinel-1 Level-1 Ground Range Detected (GRD) imagery has already undergone the following preprocessing steps (Fig. 2):

1) Apply-orbit-file (updates orbit metadata)
2) ARD (Analysis-Ready-Data) border noise removal (removes low intensity noise and invalid data on the scene edges)
3) Thermal noise removal (removes additive noise in sub-swaths)
4) Radiometric calibration (computes backscatter intensity using sensor calibration parameters)
5) Terrain-correction (orthorectification)
6) Conversion of the backscatter coefficient into decibels (dB) according to the equation 1:

$$\sigma^\circ = 10 * log10\sigma^\circ , \quad (1)$$

where σ° = backscatter coefficient

Additionally, a speckle filter is implemented during processing with a smoothing radius of 50 m to minimize the impact of granular noise. Speckles are inherent in SAR imagery that can affect the quality of the image and pose challenges in feature interpretation. The occurrence of speckles is due to the coherent nature of the radar signal used in SAR imaging.

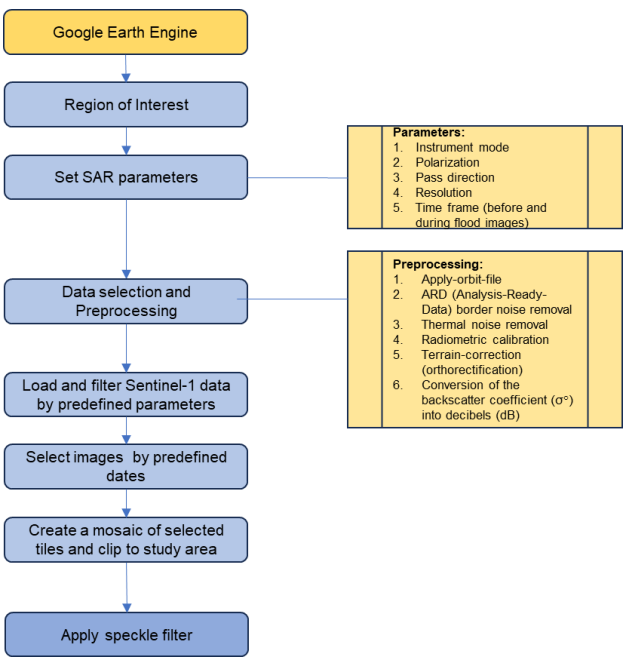

Figure 2. Data selection and preprocessing of Sentinel-1 SAR images in Google Earth Engine.

2.3.3 Change detection: To determine the changes resulting from flooding, a straight-forward change detection approach is employed. This is done by dividing the after-flood mosaic by the before-flood mosaic, to generate a raster layer showing the degree of change per pixel. A predefined threshold value for $\Delta\sigma^o$ of 1.25 dB is applied assigning 1 to all values greater than 1.25 dB (flood pixels) and a value of 0 to all values less than 1.25 dB (non-flood pixels). Through thresholding, the difference image will identify the areas that have changed significantly. In this case, a binary raster layer will be created showing the potential flood extent. High values, depicted by bright pixels, indicate significant change, whereas lower values represented by dark pixels suggest little change. The threshold of 1.25 dB has been chosen in this study through trial and error. However, it can be varied in case of high rates of false positive or false negative values.

2.3.4 Refining the flood extent layer: Supplementary datasets were also employed to remove false positives in the flood extent layer. The JRC Global Surface Water dataset was utilized to exclude areas submerged for over 10 months annually. This dataset also provides the spatial and temporal distribution of surface water, covering 1984 to 2021 including statistics detailing the extent and variability of these water surfaces (Pekel et al., 2016). The dataset also provided a spatial resolution of 30 m.

In order to exclude areas with a slope exceeding 5%, a digital elevation model (WWF HydroSHEDS v1) is also used, which is based on elevation data acquired in 2000 through NASA's Shuttle Radar Topography Mission (SRTM). This dataset has a spatial resolution of 3 arc-seconds or ~90 m (Lehner and Grill, 2013; Lehner et al., 2008).

Furthermore, an evaluation of the connectivity of the flood pixels is also conducted to eliminate those connected to eight or fewer neighbours. Assessing the connectivity of flood pixels is essential to reduce noise in the data. This ensures that only meaningful and coherent flood patterns are considered. This process will further reduce the noise of the produced flood extent.

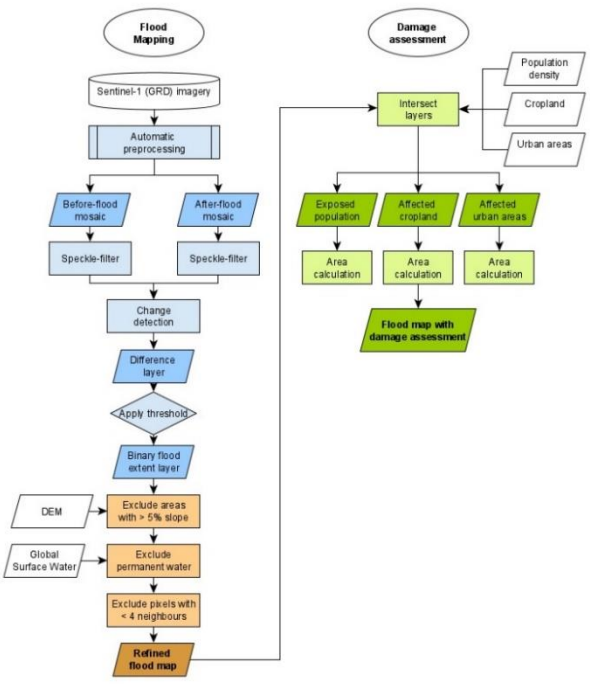

Figure 3. Flood Mapping and Damage Assessment workflow using Sentinel-1 in Google Earth Engine (UN SPIDER, 2019).

2.3.5 Area calculation of flood extent: To delineate the extent of the flood area, a raster layer was created within the refined flood extent map. This layer will be used to calculate the area in square meters for each pixel while considering the appropriate map projection. By adding up all the pixel values, the total area information can be obtained and subsequently converted into hectares. The output will be conveniently displayed on the 'Results' panel, located in the bottom-left corner of the Map Viewer interface of the Google Earth Engine (Fig. 5).

2.4 Assessment and Mapping of affected cropland, urban areas, and exposed population

2.4.1 Exposed population density: To obtain an estimate of the number of exposed populations, this study used the 2020 population density map of UN OCHA with 30-m resolution (Facebook Connectivity Lab and CIESIN – Columbia University, 2016). The dataset provides information on the population residing in each raster cell. To intersect the flood layer with the population layer, the flood extent raster underwent resampling and reprojection to match the population dataset. Following this, an intersection between the two layers is computed, resulting in a new raster layer. To determine the population at risk, values of each pixel of the exposed population raster are summed up and displayed in the 'Results' panel of the Map Viewer (Fig. 7).

2.4.2 Affected cropland: To determine the affected cropland, this study utilized the 2020 Land Cover Map (LCM) produced by the National Mapping and Resource Information Authority (NAMRIA) of the Department of Environment and Natural Resources (DENR). This dataset was converted into a raster format and the land cover classes from the LCM were used as bands to extract the specific land cover class needed for our analysis.

The LCM produced by DENR-NAMRIA contains the spatial location, extent, and distribution of various land cover types. It was derived through digital interpretation of Sentinel-2 satellite imagery obtained from the European Space Agency (ESA) between 2017 and 2018. The imagery has a high spatial resolution of 10 meters, allowing for detailed analysis of land cover patterns. The Sentinel-2 was processed based on the 12 land cover categories, namely, Closed Forest, Open Forest, Mangrove Forest, Brush/Shrubs, Grassland, Perennial Crop, Annual Crop, Open/Barren, Built-up, Marshland/Swamp, Fishpond, and Inland Water. These categories were further divided into subclasses to provide more specific information on land cover characteristics. In total, there are 21 classes that can be identified, with two separate classes dedicated to cropland: 'class 16' for Annual Crop and 'class 17' for Perennial Crop. Both categories are obtained from the dataset and overlaid onto the flood extent layer, which has been resampled to match the scale and projection of the LCM of DENR-NAMRIA. The affected cropland area is computed using the same method as the flood extent and presented in the 'Results' panel.

2.4.3 Affected urban areas: The total affected urban areas are calculated in the same manner as the previous, utilizing the NAMRIA 2020 Land Cover Map. 'Class 20,' denoted as the Built-up area in the LCM is extracted to assess potentially affected urban areas. However, in this process, there is a high likelihood that affected urban areas may be underestimated, due to difficulties of properly detecting water in built-up areas.

3. RESULTS AND DISCUSSION

3.1 Results

3.1.1 Rapid Flood Mapping and Damage Assessment: The resulting map of the rapid flood mapping and damage assessment is shown in Fig. 4. The results panel (lower left side) summarized the details of the damage assessment–flooding dates, estimated flood extent area, estimated number of exposed people, estimated cropland area, estimated urban area, as well as the percentages affected out of the total number of people or area. The inset map in Fig. 4 below also shows the map focused on Tuguegarao City, to better visualize the exposed population and affected urban area, since these are not that visible in the provincial level view.

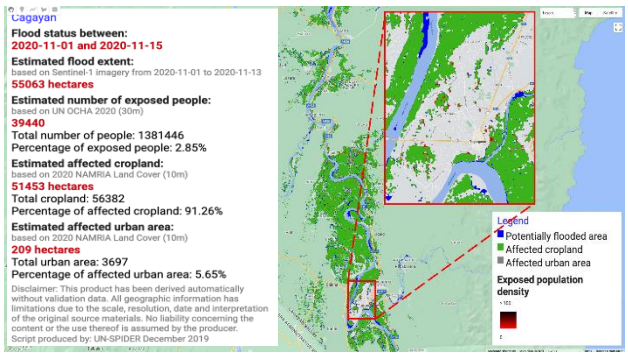

Figure 4. Rapid flood mapping and damage assessment in Cagayan

3.1.2 Potentially flooded area: The potentially flooded area in the province of Cagayan is displayed in blue color in Fig. 5. The results panel on the lower left side of the figure, shows the name of the province, the before- and end-dates where the flooding occurred, and the estimated flood extent area in the province.

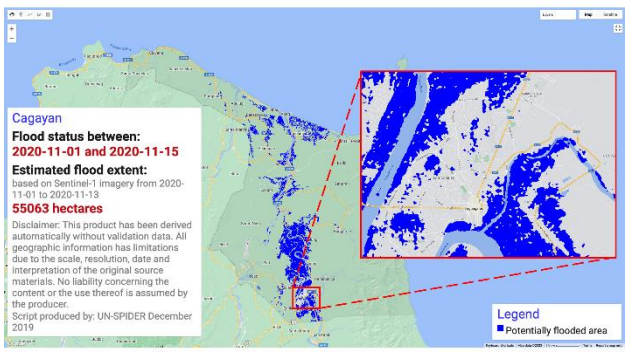

Figure 5. Potentially flooded area in Cagayan

Among all the provinces evaluated in this study, Cagayan has the largest estimated flood extent area. Shown in Table 3 is the summary of the estimated flood extent area per province.

Province	Estimated flood extent (ha)
Cagayan	55,063
Isabela	38,214
Camarines Sur	19,959
Albay	1, 651

Table 3. Summary of estimated flood extent area per province

3.1.3 Impact of flooding on Cropland and Urban areas: To evaluate the impact of the flooding on croplands, the annual and perennial crop classes were extracted from the NAMRIA LCM. Similarly, the built-up class was extracted from the LCM to obtain the urban area.

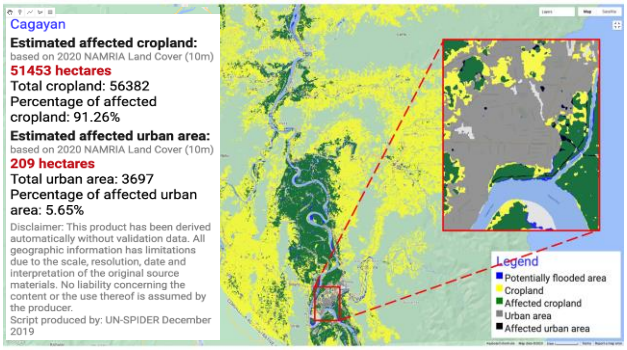

Figure 6. Impact of the flooding on the cropland and urban area

On Fig. 6, the impact of the flooding on the cropland and urban area in Cagayan is presented. The intersection between the total cropland (in yellow) and the potentially flooded area (in blue) was extracted to obtain the potentially affected croplands (in green). Likewise, the intersection between the total urban area (in grey) and the potentially flooded area was extracted to obtain the potentially affected urban areas (in black).

The affected cropland and urban areas (in ha) per province, as well as the percentage of the affected over the total area, is summarized in Table 4.

Province	Affected cropland area in ha (% of affected over total)	Affected urban area in ha (% of affected over total)
Cagayan	51,453 (91.26%)	209 (5.65%)
Isabela	35,919 (47.72%)	134 (3.30%)
Camarines Sur	19,367 (32.21%)	269 (6.38%)
Albay	1,022 (3.52%)	4 (0.26%)

Table 4. Affected cropland and urban areas per province.

3.1.4 Impact of the flooding on the population: The damage assessment also includes the evaluation of the impact of the flooding on the population per province. Population density data was intersected with the potentially flooded area to extract the exposed population density. Fig.7 shows the impact of the flooding on the population of Cagayan, including an inset map to highlight Tuguegarao City.

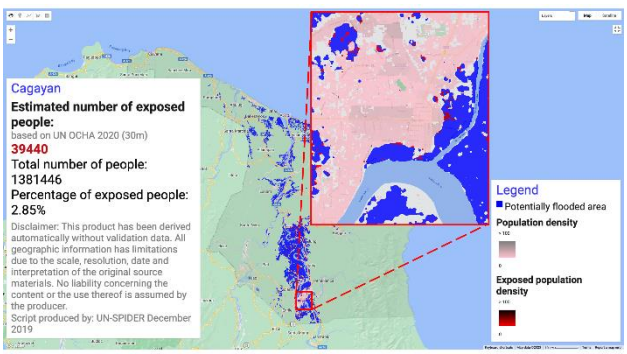

Figure 7. Population affected by flooding in Cagayan province (inset: Tuguegarao City).

The total number of people and the exposed population density are summarized in Table 5. The percentage of the exposed population over the total number of people per province are also shown in Table 5.

Province	Population density	Exposed population density (% of exposed over total)
Cagayan	1,381,446	39,440 (2.85%)
Isabela	1,903,327	19,313 (1.01%)

Camarines Sur	2,441,719	23,726 (0.97%)
Albay	1,471,111	664 (0.05%)

Table 5. Summary of the population density and exposed population per province

3.2 Discussion

3.2.1 Strengths and limitations of Rapid flood mapping and damage assessment using GEE: Our proposed approach was derived from the recommended practice of UN SPIDER. The said approach was to offer a rapid and user-friendly tool for generating information on flood extent, as well as the impact on cropland and population density, catering to users with varying levels of expertise (UN SPIDER, 2019). To ensure precise and localized information, this study explores updated and alternative datasets specifically for damage assessment. Additionally, this approach was implemented in this study as a use case in the Philippines.

The integration of localized datasets into the proposed rapid flood mapping and damage assessment workflow using Google Earth Engine has introduced several strengths, making it a valuable tool for flood monitoring and assessment. The following are the observed strengths:

1. *Workflow can be adaptable for use in various areas.* The workflow is designed to be easily implemented to different areas by simply identifying the area and period of event. This flexibility allows for the adaptation of the methodology to various regions, making it applicable for flood mapping and damage assessment in different geographical contexts.
2. *Enhanced Accuracy.* By incorporating localized datasets, the accuracy of flood mapping and damage assessment is improved. The inclusion of region-specific data allows for more precise identification and delineation of flooded areas, leading to more accurate results.
3. *Automation is possible after identification of area and period of event.* Once the area of interest and time periods are specified, the workflow can be automated. This automation streamlines the process and reduces the manual effort required for flood mapping and damage assessment, enabling efficient analysis even for large-scale areas.
4. *Minimal processing time.* The workflow demonstrates minimal processing time, a crucial for rapid flood mapping and damage assessment. With the efficient algorithms and computational capabilities of Google Earth Engine, this allows to the rapid generation of flood extent maps and assessment outputs, enabling near-real-time monitoring and reporting of flood events.
5. *Cloud independent monitoring of flood event.* The use of SAR data in Google Earth Engine enables cloud-independent flood monitoring. SAR sensors can penetrate clouds, providing consistent and reliable data even during cloudy conditions, which is particularly advantageous for regions such as Philippines with frequent cloud cover.
6. *Cloud-processing enables the incorporation of additional datasets for defining the flood extent (e.g., DEM and global water mask).* By utilizing cloud processing, the workflow can incorporate auxiliary datasets such as digital elevation models (DEMs) and global water masks. These additional datasets help in accurately delineating the flood extent and provide contextual information for improved flood mapping and damage assessment. However, it still important to note that careful selection and validation of these datasets are still essential to ensure their suitability for the specific analysis area and flood event being assessed.
7. *Offers supplementary information on exposed population, affected cropland and urban areas.* The developed workflow allows to identification and display information on the impact of flooding on cropland and population centers as well as the flood-affected areas ranging from barangays (local communities) to provinces. This analysis helps address the significant concerns arising from the flooding event.

Despite the strengths, the workflow also has certain limitations that should be taken into consideration. These limitations have been also identified by the UN SPIDER (2019) as follows:

1. *Detection of false positives from changes on the land surface unrelated to flooding.* One limitation of the workflow is the potential for false positives resulting from changes on the land surface that are unrelated to flooding. Various factors, such as land use changes or human activities, can generate similar radar responses as floods, leading to misinterpretations (Notti et al., 2018). This emphasizes the need for careful validation and ground truthing to differentiate actual flood extents from other surface changes.
2. *Difficulties of delineating flood extent in urban or densely vegetated areas.* SAR signals can be attenuated or scattered by buildings, infrastructure, and dense vegetation, making it difficult to differentiate flooded areas from other features (Refice et al., 2018). This limitation may affect the accuracy of flood extent mapping in such areas (Tay et al., 2020).
3. *Inability to capture flood peaks due to the frequency of acquisition of Sentinel-1.* The frequency of acquisition of Sentinel-1 SAR data, which is utilized in the workflow, may not capture the flood peak for every event. Depending on the revisit time and availability of SAR acquisitions, it might not be possible to precisely capture the highest extent of the flood, especially for rapidly changing flood events (Notti et al., 2018). This difficulty makes it challenging to incorporate into real-time hazard analysis (Tiampo et al., 2022).
4. *False positives caused by the relative orbits.* Differences in the relative orbits of SAR acquisitions can lead to false positives in flood mapping. Inconsistencies between overlapping SAR images acquired at different times or from different paths can introduce errors in flood extent delineation, particularly at the borders of the analyzed area (Berezowski et al., 2020).
5. *Border noise errors (when processing large areas).* Processing large areas with SAR data can introduce border noise errors. The transition zone between neighboring SAR scenes can be affected by artifacts or inconsistencies, leading to errors in flood extent mapping near the borders of the analyzed area (Ali et al., 2018). Careful data selection and processing techniques are necessary to minimize these errors.

Understanding the strengths and limitations of the proposed methodology for rapid flood mapping and damage assessment workflow using Google Earth Engine helps to provide a comprehensive view of its advantages and disadvantages. By leveraging its strengths and addressing its limitations, the workflow can be further improved and tailored to meet the specific needs of flood monitoring and assessment in different regions.

3.2.2 Comparative Flood Inundation

In 2020, NAMRIA was able to generate a flood extent map of Cagayan and Isabela province along the Cagayan River, after the Typhoon Ulysses flood event. In Fig. 8, the red color represents the NAMRIA flood extent map, whereas the green color represents the GEE-generated flood map. The overlap between the two flood maps is presented in the blue color. Through visual comparison, there is a significant amount of overlap between the

two maps. However, comparing the two maps quantitatively, the overlap between them is only 52.68%.

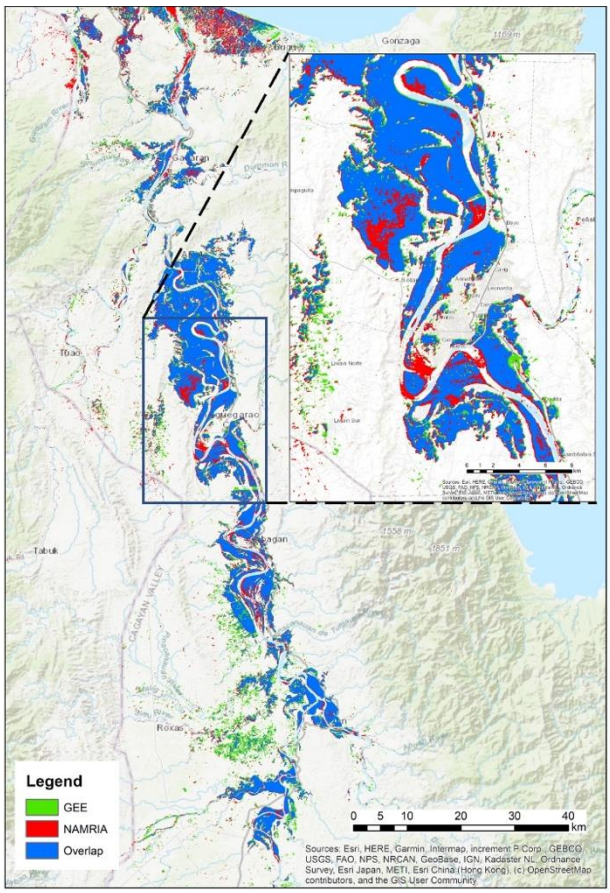

Figure 8. Comparing the GEE-generated and NAMRIA flood extent maps

The variations in flood extent may be attributed to several factors, including the parameters used (e.g., 1.25 dB as threshold value for $\Delta\sigma^o$). The threshold value may affect the classification of the flooded areas, depending on the difference between pixels from the different images (Martinis et al., 2009). Another factor would be the differences in the time periods of satellite images used for the pre- and post-flooding, which may capture changes in water levels and other conditions. Supplementary datasets, such as water masks and digital elevation models (DEMs), and the specific approach employed to refine the flood extent determination may also be sources of discrepancy between the two flood extent maps. These factors collectively contribute to the differences observed in the flood extent maps, highlighting the need to carefully consider and evaluate each parameter, period of image acquisition, and supplementary datasets to ensure accurate and reliable outputs.

4. CONCLUSION

The study successfully demonstrated the application of Google Earth Engine to rapidly generate SAR-derived flood extent maps and conduct damage assessments in regions affected by Typhoons Goni and Vamco, specifically in the provinces of Cagayan, Isabela, Camarines Sur, and Albay. The analysis yielded significant insights on flood extent and damages offering crucial information for disaster response and preparedness efforts. Cagayan province was estimated to experience the largest inundated area covering approximately 55,063 hectares. This province also had the largest population at risk, with around 39,440 individuals who were potentially exposed to the effects of flooding. Moreover, croplands in Cagayan province experienced the most substantial impact (~91.26% of croplands) due to the swelling of the Cagayan River. Camarines Sur experienced severe devastation in urban areas, with about 269 hectares affected by flooding from the Bicol River.

By using localized datasets such as land cover maps from DENR-NAMRIA and population density maps from UN OCHA, flood mapping and damage assessment processes improved significantly. This integration of detailed and localized information led to more accurate results. The population density map offered insights on the estimated number of people affected by floods, which is crucial for emergency response planning and resource allocation. Additionally, the utilization of land cover maps facilitated the identification of inundated cropland areas, assessment of its impact on agricultural production, and understanding the corresponding potential food security implications. The workflow offers several strengths, including its replicability to different regions, potential for automation, and rapid assessment enabled by GEE. Despite its strengths, the proposed methodology may be further improved by integrating optical imagery with SAR data for more accurate flood detection. For future studies, it is recommended to include valuation of damage (in monetary units) of affected agricultural crops and infrastructure. Validation is also important through comparison of outputs with that of other methods and inclusion of additional ground truth data. Furthermore, conducting sensitivity analysis will also assess robustness to variations in the parameters applied and identify areas for improvement.

ACKNOWLEDGEMENT

The authors wish to extend their gratitude to the National Mapping and Resource Information Authority (NAMRIA) under the Department of Environment and Natural Resources (DENR) for providing the 2020 Land Cover Map.

REFERENCES

Ali, I., Cao, S., Naeimi, V., Paulik, C., Wagner, W., 2018. Methods to remove the border noise from Sentinel-1 Synthetic Aperture Radar data: implications and importance for time-series analysis. *IEEE Journal of Selected Topics in Applied Earth Observations and Remote Sensing*, *11*(3), 777–786. https://doi.org/10.1109/jstars.2017.2787650.

Berezowski, T., Bieliński, T., Osowicki, J., 2020. Flooding extent mapping for synthetic aperture radar time series using river gauge observations. *IEEE Journal of Selected Topics in Applied Earth Observations and Remote Sensing*, *13*, 2626–2638. https://doi.org/10.1109/jstars.2020.2995888.

Department of Environment and Natural Resources - River Basin Control Office (DENR-RBCO), 2015. Formulation of an Integrated Bicol River Basin Management Plan Executive Summary Vol. 1. https://rbco.denr.gov.ph/masterplans/bicolexecutivesummary.pdf (01 June 2023).

Facebook Connectivity Lab and Center for International Earth Science Information Network - CIESIN - Columbia University. 2016. High Resolution Settlement Layer (HRSL). data.humdata.org/dataset/philippines-high-resolution-population-density-maps-demographic-estimates (05 May 2023).

Franceschetti, G., Lanari, R., 2018. Synthetic Aperture Radar processing. *CRC Press eBooks*. doi.org/10.1201/9780203737484.

Gorelick, N., Hancher, M., Dixon, M. J., Ilyushchenko, S., Thau, D., Moore, R., 2017. Google Earth Engine: Planetary-scale geospatial analysis for everyone. Remote Sensing of Environment, 202, 18–27. doi.org/10.1016/j.rse.2017.06.031.

International Federation of Red Cross and Red Crescent Societies (IFRC). 2021a, March 8. *Philippines: Floods and Typhoons 2020 (Typhoon Goni) Operation Update Report n° 3, DREF Operation n° MDRPH041 - Philippines*. ReliefWeb. reliefweb.int/report/philippines/philippines-floods-and-typhoons-2020-typhoon-goni-operation-update-report-n-3 (08 May 2023).

International Federation of Red Cross and Red Crescent Societies (IFRC). 2021b, September 25. *Philippines: Typhoon Vamco Final Report, DREF Operation n° MDRPH042 - Philippines*. ReliefWeb. reliefweb.int/report/philippines/philippines-typhoon-vamco-final-report-dref-operation-n-mdrph042 (08 May 2023).

Islam, M. T., & Meng, Q., 2022. An exploratory study of Sentinel-1 SAR for rapid urban flood mapping on Google Earth Engine. *International Journal of Applied Earth Observation and Geoinformation*, *113*, 103002. doi.org/10.1016/j.jag.2022.103002.

Lehner, B., Grill, G., 2013. Global river hydrography and network routing: baseline data and new approaches to study the world's large river systems. *Hydrological Processes*, *27*(15), 2171–2186. doi.org/10.1002/hyp.9740.

Lehner, B., Verdin, K. L., Jarvis, A., 2008. New global hydrography derived from spaceborne elevation data. *Eos, Transactions American Geophysical Union*, *89*(10), 93. doi.org/10.1029/2008eo100001.

Martinis, S., Twele, A., Voigt, S., 2009. Towards operational near real-time flood detection using a split-based automatic thresholding procedure on high resolution TerraSAR-X data. *Natural Hazards and Earth System Sciences*, *9*(2), 303–314. doi.org/10.5194/nhess-9-303-2009.

Marzano, F. S., Mori, S., Weinman, J., Montopoli, M., 2012. Modeling polarimetric response of spaceborne synthetic aperture radar due to precipitating clouds from X- to Ka-Band. *IEEE Transactions on Geoscience and Remote Sensing*, *50*(3), 687–703. doi.org/10.1109/tgrs.2011.2163942.

Nghia, B. T., Pal, I., Chollacoop, N., Mukhopadhyay, A., 2022. Applying Google earth engine for flood mapping and monitoring in the downstream provinces of Mekong River. *Progress in Disaster Science*, *14*, 100235. doi.org/10.1016/j.pdisas.2022.100235.

Notti, D., Giordan, D., Calò, F., Pepe, A., Zucca, F., Galve, J. P., 2018. Potential and limitations of open satellite data for flood mapping. *Remote Sensing*, *10*(11), 1673. doi.org/10.3390/rs10111673.

O'Grady, D., LeBlanc, M. E., Gillieson, D., 2011. Use of ENVISAT ASAR Global Monitoring Mode to complement optical data in the mapping of rapid broad-scale flooding in Pakistan. *Hydrology and Earth System Sciences*, *15*(11), 3475–3494. doi.org/10.5194/hess-15-3475-2011.

Pekel, J., Cottam, A., Gorelick, N., Belward, A., 2016. High-resolution mapping of global surface water and its long-term changes. *Nature*, *540*(7633), 418–422. doi.org/10.1038/nature20584.

Pralle, S., 2018. Drawing lines: FEMA and the politics of mapping flood zones. *Climatic Change*, *152*(2), 227–237. doi.org/10.1007/s10584-018-2287-y.

Principe, J., 2012. Exploring climate change effects on watershed sediment yield and land cover-based mitigation measures using SWAT Model, RS and GIS: Case of Cagayan River Basin, Philippines. *The International Archives of the Photogrammetry, Remote Sensing and Spatial Information Sciences*, *XXXIX-B8*, 193–198. doi.org/10.5194/isprsarchives-xxxix-b8-193-2012.

Principe, J., Blanco, A., 2012. Integrated Use of Remote Sensing, GIS and SWAT Model to Explore Climate Change Effects on River Discharge in the Cagayan River Basin and Land Cover-based Adaptation Measures. *33rd Asian Conference on Remote Sensing*. a-a-r-s.org/proceeding/ACRS2012/Proceeding%20ACRS%202012/Technical%20Sessions/F3%20Other%20(3)/F3-4.pdf.

Refice, A., D'Addabbo, A., Capolongo, D., 2018. Flood monitoring through remote sensing. In *Springer Remote Sensing/Photogrammetry*. doi.org/10.1007/978-3-319-63959-8.

Schumann, G., Bates, P. D., Horritt, M. S., Matgen, P., Pappenberger, F., 2009. Progress in integration of remote sensing–derived flood extent and stage data and hydraulic models. *Reviews of Geophysics*, *47*(4). doi.org/10.1029/2008rg000274.

Tamiminia, H., Salehi, B., Mahdianpari, M., Quackenbush, L. J., Adeli, S., Brisco, B., 2020. Google Earth Engine for geo-big data applications: A meta-analysis and systematic review. *ISPRS Journal of Photogrammetry and Remote Sensing*, *164*, 152–170. doi.org/10.1016/j.isprsjprs.2020.04.001.

Tay, C. S., Yun, S., Chin, S. T., Bhardwaj, A., Jung, J., Hill,b E. M., 2020. Rapid flood and damage mapping using synthetic aperture radar in response to Typhoon Hagibis, Japan. *Scientific Data*, *7*(1). doi.org/10.1038/s41597-020-0443-5.

Tiampo, K. F., Huang, L., Simmons, C., Woods, C., Glasscoe, M., 2022. Detection of flood extent using Sentinel-1A/B Synthetic Aperture Radar: an application for hurricane Harvey, Houston, TX. *Remote Sensing*, *14*(9), 2261. doi.org/10.3390/rs14092261.

Torres, R., Snoeij, P., Geudtner, D., Bibby, D. F., Davidson, M., Attema, E., Potin, P., Rommen, B., Floury, N., Brown, M., Traver, I. N., Deghaye, P., Duesmann, B., Rosich, B., Miranda, N., Bruno, C., L'Abbate, M., Croci, R., Pietropaolo, A., . . . Rostan, F., 2012. GMES Sentinel-1 mission. *Remote Sensing of Environment*, *120*, 9–24. doi.org/10.1016/j.rse.2011.05.028.

United Nation Office for the Coordination of Humanitarian Affairs (UN OCHA), 2020, November 26. *Philippines: Super Typhoon Goni (Rolly) and Typhoon Vamco (Ulysses) Humanitarian Needs and Priorities (Nov 2020 - April 2021) - Philippines*. ReliefWeb. reliefweb.int/report/philippines/philippines-super-typhoon-goni-rolly-and-typhoon-vamco-ulysses-humanitarian-needs (02 May 2023).

United Nations Platform for Space-based Information for Disaster Management and Emergency Response (UN SPIDER), 2019. *Step-by-Step: Recommended Practice: Flood Mapping and Damage Assessment Using Sentinel-1 SAR Data in Google Earth Engine*. UN SPIDER Knowledge Portal. un-spider.org/advisory-support/recommended-practices/recommended-practice-google-earth-engine-flood-mapping/step-by-step (01 March 2023).

University of the Philippines Los Baños - College of Forestry and Natural Resources (UPLB-CFNR), 2018. *Climate Responsive Integrated Master Plan for Cagayan River Basin*. Department of Environment and Natural Resources - River Basin Control Office (DENR-RBCO). riverbasin.denr.gov.ph/masterplans/cagayanexecutivesummary.pdf (01 June 2023).

Voigt, S., Kemper, T., Riedlinger, T., Kiefl, R. F., Scholte, K., Mehl, H., 2007. Satellite image analysis for disaster and crisis-management support. *IEEE Transactions on Geoscience and Remote Sensing*, *45*(6), 1520–1528. doi.org/10.1109/tgrs.2007.895830.

APPENDIX

The code for the Rapid Flood Mapping and Damage Assessment implementation on Google Earth Engine can be viewed in this link:https://code.earthengine.google.com/7beb788c965b6a7c99fbcc34db18f385